# Onset of thermovibrational filtration convection: Departure from thermal equilibrium

S. Saravanan* and T. Sivakumar
*Department of Mathematics, Bharathiar University, Coimbatore 641 046, Tamil Nadu, India*
(Received 2 November 2010; revised manuscript received 8 July 2011; published 8 August 2011)

A theoretical investigation is made to understand the onset of thermovibrational convection in a fluid saturated horizontal porous layer subjected to isothermal heating either at the bottom or at the top. Attention is paid to the situation in which the solid and fluid phases of the porous medium may fail to obey thermal equilibrium locally. Vertical harmonic vibrations of arbitrary amplitude and frequency are considered. The threshold for dynamic instability is found via synchronous and subharmonic resonant modes exploiting the Floquet theory. The nonequilibrium effect is felt only for intermediate values of the interphase heat transfer coefficient $H$. It is found that $H$ restrains the onset of convection whereas $\gamma$, the porosity modified conductivity ratio, encourages it. $\gamma$ constricts the convective cells ensuing at the threshold except when the layer heated from below is undergoing small amplitude vibrations. Small values of $\gamma$ expose the competition between synchronous and subharmonic modes for a wider range of vibrational frequencies.

DOI: 10.1103/PhysRevE.84.026307 PACS number(s): 47.20.−k, 44.30.+v, 46.40.−f

## I. INTRODUCTION

The widely studied configurations in hydrodynamics exhibiting pattern forming instabilities are a fluid layer with an imposed adverse vertical temperature gradient (Rayleigh Bénard convection [1,2]) and a vertically oscillated open dish of fluid (Faraday surface waves [3]). For sufficiently weak driving mechanisms, both the systems are in macroscopically time-independent uniform states. As the driving is increased, regular spatial variations appear at well established thresholds and the dynamics becomes complex in space and time.

Controlling natural buoyancy flow arising in the Rayleigh-Bénard setup is essential in certain situations, like fabricating extremely pure materials. One of the ways to achieve this is to introduce vertical vibrations that can stabilize the adverse density stratification in a horizontal fluid layer heated from below, as in the case of an inverted pendulum. This analogy was first noticed theoretically [4,5] and stimulated theoretical [6,7] and experimental [8–10] research on thermovibrational convection. The externally imposed mechanical vibrations impart a fluctuating component to the already existing static gravity and produce a convective flow component oscillating with time. In this paper, we report the onset of convection in a vertically vibrating fluid saturated porous layer.

The extensive work done so far on convective instability in porous media with constant gravity has been well reviewed [11]. In most of these investigations, the state of local thermal equilibrium (LTE) was profoundly employed. Nevertheless, in many practical applications involving sudden and high speed flows, the hot fluid stream penetrates well into the relatively cold porous structures and hence in a representative elementary volume its temperature becomes sufficiently higher than that of the adjacent solid phase. This local thermal nonequilibrium (LTNE) situation can be handled by considering separate energy equations for solid and fluid phases with a coupling in between them to represent the energy exchange. Nield and Bejan [11] introduced one of the simplest models to deal with the LTNE situation. A brief review of various two equation models accounting the LTNE effect in porous convection and many recent studies including free and external forced convection boundary layers were given by Rees and Pop [12]. The onset criterion for convection in a porous medium with the LTNE effect was first determined by Banu and Rees [13]. They predicted the emergence of tall thin convection cells in the LTNE situation under circumstances that depend on the conductivity ratio of the two phases. This was followed by similar studies in the Brinkman porous medium confined between stress-free [14,15] and rigid [16] boundaries. All the above studies were performed based on linear stability analysis, while Straughan [17] made a nonlinear analysis and concluded that the linear results are important as they coincide with the nonlinear limits. The recent works pertaining to the LTNE effects have concentrated on various themes and combined effects like rotation, heat generation, density inversion, applied pressure gradient, nanofluid, etc. [18–22].

The published works on thermovibrational convection in porous media are quite recent and fairly limited [23,24]. There are also few recent works available in the literature dealing with thermovibrational convection in a more general Brinkman porous medium [24–26]. In our recent study [24], thermovibrational convection in a Brinkman porous layer in the presence of vibrations of arbitrary amplitude and frequency was considered. It was demonstrated that the vibration amplitude could either favor or suppress setting up of convection depending on the vibration frequency for a layer heated from below, whereas it always favors convection irrespective of the values of frequency for the layer heated from above. To the best of our knowledge, there seems to have been no work on the stability analysis of thermovibrational convection wherein the LTE assumption breaks down. Hence we study the onset of convection in a vertically vibrating porous layer exhibiting thermal nonequilibrium. Moreover, though there are several studies related to time-dependent gravity modulation in both fluid and porous domains, most of them do not report their results to a wider range of vibrating parameters. Because of the limitations of the adopted solution procedures, their investigations were restricted to either small amplitude [25,27] or low frequency [28] or high frequency [29]. Therefore, we

*sshravan@lycos.com

 

are also interested in predicting the results for an arbitrary range of frequency and amplitude using an efficient procedure, viz., continued fraction method [30], that does not impose any constraint on the vibrating parameters.

## II. MATHEMATICAL FORMULATION

We consider a sparsely packed, isotropic, and homogeneous porous layer saturated with a viscous incompressible fluid. We assume that the layer and its boundaries are subjected to vertical harmonic vibration. The layer is confined between two horizontal planes of infinite extent $z = 0$ and $z = h$, which are maintained at temperatures $T_1$ and $T_2$, respectively. A Cartesian coordinate system is chosen with its origin in the lower plane and the $z$ axis pointing vertically upward. Here the characteristic temperature difference $\Delta T = T_1 - T_2$ is positive for the case of unstable equilibrium (layer heated from below), while it is negative for the stable equilibrium (layer heated from above). The porous medium need not be consistent with the LTE condition. Brinkman's law is used to model the flow through it after neglecting inertial effects.

The appropriate equations governing laminar flow through the porous medium under the Oberbeck-Boussinesq approximation are

$$\frac{1}{\varphi}\frac{\partial \mathbf{v}}{\partial t} + \frac{1}{\varphi^2}\mathbf{v}\cdot\nabla\mathbf{v} = -\frac{1}{\rho}\nabla p - \frac{\nu}{K}\mathbf{v} + \nu\nabla^2\mathbf{v} + \beta T_f g(t)\widehat{\mathbf{k}}, \tag{1}$$

$$\varphi(\rho c_p)_f \frac{\partial T_f}{\partial t} + (\rho c_p)_f \mathbf{v}\cdot\nabla T_f = \varphi k_f \nabla^2 T_f + \overline{H}(T_s - T_f), \tag{2}$$

$$(1-\varphi)(\rho c_p)_s \frac{\partial T_s}{\partial t} = (1-\varphi)k_s\nabla^2 T_s - \overline{H}(T_s - T_f), \tag{3}$$

$$\nabla\cdot\mathbf{v} = 0, \tag{4}$$

where $\mathbf{v} = (v_1, v_2, v_3)$ is the filtration velocity, $p$ the pressure, $\varphi$ the porosity, $K$ the permeability, $\rho$ the density, $\nu$ the kinematic viscosity, $\beta$ the thermal expansion coefficient, and $\widehat{\mathbf{k}}$ the unit vector directed vertically upward. Also, $c_p$ is the specific heat, $k$ the thermal conductivity, $T$ the temperature with the subscripts $f$ and $s$ denoting fluid and solid phases, respectively, and $\overline{H}$ the interphase heat-transfer coefficient. The time-dependent gravitational field is taken to be $g(t) = g_0 + \frac{A}{\varphi}\Omega^2 f''(\tau)$, where $g_0$ is a reference acceleration level, $A$ the vibration amplitude, $\Omega$ the vibration frequency, and $f(\tau)$ the $2\pi$-periodic function with zero $2\pi$ average.

Equation (1) contains Brinkman's viscous term, which creates a thin boundary layer with thickness of order $\sqrt{K}$, where $K$ is the permeability of the porous medium. One can also notice that Eqs. (2) and (3) are coupled together through an additional term that incorporates the energy exchange between the two phases when the porous medium exhibits a thermal nonquilibrium behavior. One may note that in the absence of fluid flow, these equations take the form of Fourier's equation with additional source-sink terms, which allow the microscopic transfer of heat between the phases due to differences in their local intrinsic values. It is assumed that, at the bounding surfaces, the solid and fluid phases have identical temperatures which would settle, for the time being, the question of appropriate boundary conditions for the temperature fields in the absence of LTE [15]. The bounding surfaces are flat and stress-free and obey the conditions

$$v_3 = \frac{\partial v_1}{\partial z} = \frac{\partial v_2}{\partial z} = 0, \quad T_f = T_s = T_1 \quad \text{at} \quad z = 0, \tag{5}$$

$$v_3 = \frac{\partial v_1}{\partial z} = \frac{\partial v_2}{\partial z} = 0, \quad T_f = T_s = T_2 \quad \text{at} \quad z = h. \tag{6}$$

We consider a quasiequilibrium state in which the mean velocity is zero, though the oscillating velocity is nonzero. Accordingly, we seek solutions in the form $\mathbf{v} = \mathbf{v}^0$, $T_f = T_f^0(z)$, $T_s = T_s^0(z)$, and $p = p^0(z,t)$. Thus Eqs. (1)–(4), together with the boundary conditions, possess the following solution:

$$\begin{aligned} \mathbf{v}^0 = 0, \quad T_f^0 = T_s^0 = T_1 - \frac{1}{h}\mathbf{\Delta} T z, \\ p^0 = \beta\rho g(t)\left(T_1 z - \frac{1}{2h}\mathbf{\Delta} T z^2\right). \end{aligned} \tag{7}$$

We study the stability of this basic state using the method of small perturbations. Let us consider the motion

$$\begin{aligned} \mathbf{v} = \mathbf{v}^0 + \mathbf{u}, \quad p = p^0 + q, \\ T_f = T_f^0 + \theta, \quad T_s = T_s^0 + \phi, \end{aligned} \tag{8}$$

where $\mathbf{u}, q, \theta$, and $\phi$ are small unsteady perturbations. Dimensionless variables are defined in terms of the length scale $h$, the time scale $h^2/\nu$, the velocity scale $\varphi\nu/h$, the pressure scale $\rho\nu^2/K$, and the temperature scale $Ch$ for both fluid and solid phases, where $C = \mathbf{\Delta} T/h$ is the basic quasiequilibrium temperature gradient. Then the nondimensional governing equations are

$$c\frac{\partial \mathbf{u}}{\partial t} = -\nabla q - \mathbf{u} + \mathrm{Da}\nabla^2\mathbf{u} + \mathrm{Gr}[1 + \eta f''(\tau)]\theta\widehat{\mathbf{k}}, \tag{9}$$

$$\frac{\partial \theta}{\partial t} - u_3 = \frac{1}{\mathrm{Pr}}\nabla^2\theta + \frac{H}{\mathrm{Pr}}(\phi - \theta), \tag{10}$$

$$\varkappa\frac{\partial \phi}{\partial t} = \frac{1}{\mathrm{Pr}}\nabla^2\phi - \frac{H\gamma}{\mathrm{Pr}}(\phi - \theta), \tag{11}$$

$$\nabla\cdot\mathbf{u} = 0, \tag{12}$$

where $\mathrm{Da} = \frac{K}{h^2}$ is the Darcy number, $\mathrm{Gr} = \frac{\beta C h^2 g_0 K}{\varphi\nu^2}$ the filtration Grashof number based on the fluid properties, $\mathrm{Pr} = \frac{\nu(\rho c_p)_f}{k_f}$ the Prandtl number, $c = \frac{\mathrm{Da}}{\varphi}$ the porosity-permeability parameter, $H = \frac{\overline{H}h^2}{\varphi k_f}$ the interphase heat-transfer coefficient, $\gamma = \frac{k_f\varphi}{k_s(1-\varphi)}$ the porosity modified conductivity ratio, $\varkappa = \frac{k_f(\rho c_p)_s}{k_s(\rho c_p)_f}$ the ratio of diffusivities, $\eta = \frac{A\Omega^2}{\varphi g_0}$ the nondimensional amplitude, and $\omega = \frac{\Omega h^2}{\nu}$ the nondimensional frequency of vibration. The nondimensional boundary conditions are

$$u_3 = \frac{\partial^2 u_3}{\partial z^2} = \theta = \phi = 0 \quad \text{at} \quad z = 0 \quad \text{and} \quad z = 1. \tag{13}$$

We then expand the vertical component of velocity and the temperature in terms of normal modes as

$$(u_3, \theta, \phi) = [\widetilde{u}_3(z,t), \widetilde{\theta}(z,t), \widetilde{\phi}(z,t)]e^{i(\alpha_1 x + \alpha_2 y)}, \tag{14}$$

where $\alpha_1$ and $\alpha_2$ represent wave numbers in the $x$ and $y$ directions, respectively. Substituting this into Eqs. (9)–(12), we obtain

$$\left[c\frac{\partial}{\partial t}+1\right](D^2-\alpha^2)\widetilde{u_3}-\mathrm{Da}(D^2-\alpha^2)^2\widetilde{u_3}+\alpha^2\mathrm{Gr}[1+\eta f''(\tau)]\widetilde{\theta}=0, \tag{15}$$

$$\frac{\partial\widetilde{\theta}}{\partial t}-\widetilde{u_3}=\frac{1}{\mathrm{Pr}}(D^2-\alpha^2)\widetilde{\theta}+\frac{H}{\mathrm{Pr}}(\widetilde{\phi}-\widetilde{\theta}), \tag{16}$$

$$\varkappa\frac{\partial\widetilde{\phi}}{\partial t}=\frac{1}{\mathrm{Pr}}(D^2-\alpha^2)\widetilde{\phi}-\frac{H\gamma}{\mathrm{Pr}}(\widetilde{\phi}-\widetilde{\theta}), \tag{17}$$

where $D=\frac{\partial}{\partial z}$ and $\alpha^2=\alpha_1^2+\alpha_2^2$ is the overall horizontal wave number. Now we separate the $z$ variable from the system (15)–(17) using the following representation:

$$[\widetilde{u_3}(z,t),\widetilde{\theta}(z,t),\widetilde{\phi}(z,t)]=[\widehat{u_3},\widehat{\theta},\widehat{\phi}](t)\sin(\pi z). \tag{18}$$

After the substitutions $t=\widehat{t}\sqrt{\mathrm{Pr}c\varkappa}$ and $\omega=\widehat{\omega}\sqrt{\mathrm{Pr}c\varkappa}$, we obtain a system of ordinary differential equations with periodic coefficients:

$$\frac{c}{r}\frac{d\widehat{u_3}}{d\widehat{t}}=-(\mathrm{Da}m^2+1)\widehat{u_3}+\frac{\alpha^2}{m^2}\mathrm{Gr}[1+\eta f''(\tau)]\widehat{\theta}, \tag{19}$$

$$\frac{1}{r}\frac{d\widehat{\theta}}{d\widehat{t}}=\widehat{u_3}-\frac{m^2}{\mathrm{Pr}}\widehat{\theta}+\frac{H}{\mathrm{Pr}}(\widehat{\phi}-\widehat{\theta}), \tag{20}$$

$$\frac{\varkappa}{r}\frac{d\widehat{\phi}}{d\widehat{t}}=-\frac{m^2}{\mathrm{Pr}}\widehat{\phi}-\frac{H\gamma}{\mathrm{Pr}}(\widehat{\phi}-\widehat{\theta}), \tag{21}$$

where $m^2=\alpha^2+\pi^2$ and $r=\sqrt{\mathrm{Pr}c\varkappa}$. We assume that $f(\tau)=\cos\omega t$ in Eq. (19) and, for notational convenience, the tilde from $\widetilde{t}$ and $\widetilde{\omega}$ will be subsequently omitted.

## III. SOLUTION: CONTINUED FRACTION METHOD

Before applying this method, first we convert Eqs. (19)–(21) into a system of algebraic equations. Following the Floquet theory, we search for the solution to the system (19)–(21) in the form

$$(\widehat{u_3},\widehat{\theta},\widehat{\phi})(t)=e^{\sigma t}\sum_{n=-\infty}^{+\infty}(w_n,\theta_n,\phi_n)e^{in\omega t}, \tag{22}$$

where the $\sigma$ is the Floquet exponent that defines the behavior of the perturbation with time. Substitution of Eq. (22) into the system (19)–(21) yields an infinite system of linear algebraic equations for determination of unknown coefficients $w_n,\theta_n,\phi_n$ :

$$\frac{2m^2}{\alpha^2\eta}\left(\frac{c}{r}(\sigma+in\omega)+1+\mathrm{Da}m^2\right)w_n=\mathrm{Gr}\left(\frac{2}{\eta}\theta_n-\theta_{n+1}-\theta_{n-1}\right), \tag{23}$$

$$\left(\frac{\mathrm{Pr}}{r}(\sigma+in\omega)+m^2+H\right)\theta_n-H\phi_n=\mathrm{Pr}w_n, \tag{24}$$

$$\left(\frac{\mathrm{Pr}\varkappa}{r}(\sigma+in\omega)+m^2+H\gamma\right)\phi_n=H\gamma\theta_n,\quad n=\ldots,-2,-1,0,1,2,\ldots. \tag{25}$$

Eliminating the variables $w_n$ and $\phi_n$ from this system, we transform it into an infinite tridiagonal system of linear algebraic equations for the coefficients $\theta_n$:

$$M_n\theta_n=-q(\theta_{n-1}+\theta_{n+1}),\quad n=\ldots,-2,-1,0,1,2,\ldots, \tag{26}$$

where

$$M_n=\left(\frac{\frac{\sigma+in\omega}{P}+1+\mathrm{Da}m^2}{P(\sigma+in\omega)+m^2+\gamma H}\right)\left[\frac{P^2}{\varkappa}(\sigma+in\omega)^2+P\left(m^2+H+\frac{m^2+\gamma H}{\varkappa}\right)(\sigma+in\omega)+m^4+m^2H+m^2\gamma H\right]-\frac{\alpha^2}{m^2}\mathrm{Ra}$$

and

$$q=\frac{\alpha^2\eta\mathrm{Ra}}{2m^2}.$$

Here $P=\sqrt{\frac{\mathrm{Pr}\varkappa}{c}}$ and $\mathrm{Ra}=\mathrm{Gr}\cdot\mathrm{Pr}$ is the Rayleigh number based on the fluid properties.

Now we use the continued fraction method to solve the above linear system. Substituting $a_n=q^nd_n$ into Eq. (26), we obtain

$$M_nd_n=-(d_{n-1}+q^2d_{n+1}),\quad n=\ldots,-2,-1,0,1,2,\ldots. \tag{27}$$

After one more substitution $\zeta_n=\frac{d_{n-1}}{d_n}$ $(d_n\neq0)$, the system (26) becomes

$$M_n=-\left(\zeta_n+\frac{q^2}{\zeta_{n+1}}\right),\quad n=\ldots,-2,-1,0,1,2,\ldots. \tag{28}$$

The validity of the transition from Eqs. (26)–(28) was discussed by Markman and Yudovich [28] and they proved that none of the coefficients $a_n$ can become zero for a solution of the system (26). From Eq. (28), using complex fractions, we derive two different recurrence relations for the unknown $\zeta_n$ as

$$\zeta_n=-M_n-\frac{q^2}{\zeta_{n+1}}=\frac{-q^2}{M_{n-1}+\zeta_{n-1}},$$

which in turn yield two different continued fractions for $\zeta_n$:

$$\zeta_n=-M_n+\cfrac{-q^2}{-M_{n+1}+\cfrac{-q^2}{-M_{n+2}+\cfrac{-q^2}{-M_{n+3}+\cdots}}}=\cfrac{-q^2}{M_{n-1}+\cfrac{-q^2}{M_{n-2}+\cfrac{-q^2}{M_{n-3}+\cdots}}}. \tag{29}$$

Assigning $n = 0$ in these leads to the following dispersion equation for the Floquet exponent $\sigma$ in the explicit form:

$$M_0 - \cfrac{q^2}{M_1 - \cfrac{q^2}{M_2 - \cfrac{q^2}{M_3 - \cdots}}} = \cfrac{q^2}{M_{-1} - \cfrac{q^2}{M_{-2} - \cfrac{q^2}{M_{-3} - \cdots}}}, \tag{30}$$

from which we can determine the values of the Floquet exponent $\sigma$.

Equation (30) is simplified to the real form when $\sigma = 0$ corresponding to the synchronous ($S$) mode with period $2\pi/\omega$, while $\sigma = i\omega/2$ corresponds to the subharmonic (SH) mode with period $4\pi/\omega$. When $\sigma = 0$, the expression for $M_n$ simplifies with the symmetry $M_{-n} = \overline{M_n}$ (the bar denotes the complex conjugate) as

$$M_n = \left(\frac{\frac{in\omega}{P} + 1 + \mathrm{Da}m^2}{in\omega P + m^2 + \gamma H}\right) \times \left[\frac{-P^2}{\varkappa} n^2\omega^2 + P\left(m^2 + H + \frac{m^2 + \gamma H}{\varkappa}\right) in\omega + m^4 + m^2 H + m^2\gamma H\right] - \frac{\alpha^2}{m^2}\mathrm{Ra}$$

and hence Eq. (30) reduces to

$$\mathrm{Re}\left(\cfrac{q^2}{M_1 - \cfrac{q^2}{M_2 - \cfrac{q^2}{M_3 - \cdots}}}\right) = \frac{M_0}{2}. \tag{31}$$

When $\sigma = i\omega/2$, the expression for $M_n$ simplifies with the symmetry $M_n = \overline{M_{n-1}}$ as

$$M_n = \left(\frac{\left(\frac{n+1}{2}\right)\frac{i\omega}{P} + 1 + \mathrm{Da}m^2}{\left(\frac{n+1}{2}\right)i\omega P + m^2 + \gamma H}\right) \times \left[\frac{-P^2}{\varkappa} n^2\omega^2 + P\left(m^2 + H + \frac{m^2 + \gamma H}{\varkappa}\right) \times \left(\frac{n+1}{2}\right) i\omega + m^4 + m^2 H + m^2\gamma H\right] - \frac{\alpha^2}{m^2}\mathrm{Ra}$$

and hence Eq. (30) becomes

$$\left|M_0 - \cfrac{q^2}{M_1 - \cfrac{q^2}{M_2 - \cfrac{q^2}{M_3 - \cdots}}}\right|^2 = q^2. \tag{32}$$

The transcendental Eqs. (31) and (32) are solved then to obtain the marginal curves of Ra against $\alpha$ for $S$ and SH modes, respectively. Prior to that, convergence of the continued fractions was verified numerically and the continued fractions were truncated once the desired precision ($10^{-4}$) is achieved. The stability characteristics, viz., the critical Rayleigh number $\mathrm{Ra}_c$, obtained by minimizing marginal Ra against $\alpha$ and the critical wave number $\alpha_c$ with the $\alpha$ corresponding to $\mathrm{Ra}_c$, are then calculated by fixing the values of other parameters.

## IV. RESULTS AND DISCUSSION

The influence of mechanical vibration on buoyancy driven convection in a fluid saturated porous medium is considered using a thermal nonequilibrium model. We can recover the results corresponding to the nonvibrating situation when $\eta = 0$, which in turn serve as the reference to which later results can be compared. By setting $\sigma = q = n = 0$ in Eq. (26), we obtain the known relation [14,15] for the Rayleigh number corresponding to the monotonic case (exchange of stabilities) of the nonvibrating situation as

$$\mathrm{Ra}_0 = \left(\frac{(\pi^2 + \alpha^2)^2}{\alpha^2} + \frac{\mathrm{Da}(\pi^2 + \alpha^2)^3}{\alpha^2}\right) \times \left(1 + \frac{H}{\pi^2 + \alpha^2 + \gamma H}\right). \tag{33}$$

Before proceeding further, let us look at the situation under two different limiting cases. Both $\mathrm{Ra}_0$ in the limit $\gamma \to \infty$ and $\mathrm{Ra}_0(\frac{\gamma}{1+\gamma})$ in the limit $H \to \infty$ become $\frac{(\pi^2+\alpha^2)^2}{\alpha^2} + \frac{\mathrm{Da}(\pi^2+\alpha^2)^3}{\alpha^2}$. At this stage, one should note that the Rayleigh number Ra defined already is based on the properties of the fluid, whereas the combination

$$\mathrm{Ra}\left(\frac{\gamma}{1+\gamma}\right) = \frac{\beta C h^2 g_0 K(\rho c_p)_f}{[\varphi k_f + (1-\varphi)k_s]\nu} \tag{34}$$

is the Rayleigh number based on the mean properties of the porous medium that is used in the equilibrium model. Thus the results of the LTE situation are recovered in both cases except a rescaling in the later. When $\mathrm{Da} \to 0$, Eq. (33) reduces to the one reported in the initial work of Banu and Rees [13] for the Darcian porous layer.

It is well known that there is no permeability-porosity relationship that can be applied universally. It is widely accepted, however, that the permeability is determined by microstructures such as pores and cracks that are connected. So one can suppose, in general, that increasing porosity results in more interconnected void spaces, which in turn contributes to higher permeability. Having this in mind, we fixed the porosities to lie in the range 0.01–0.1 for $\mathrm{Da} = 10^{-4}$ (Darcy model) and 0.1–1 for $\mathrm{Da} = 10^{-1}$ (Brinkman model). It should be noted that Da assumes values less than $10^{-3}$ for the Darcy model and exceeds $10^{-3}$ for the Brinkman model [31]. Based on these, we fixed $c$ to be $10^{-2}$ and $10^{-1}$ for the Darcy and the Brinkman models, respectively. The values of the other parameters used in this study are $\mathrm{Pr} = 1$ and $\varkappa = 1$, unless otherwise specified. This combination covers the following porous medium–fluid pairs. For air, $\mathrm{Pr} = 0.713$ at 30 °C and specific-heat capacity $(\rho C)_f = 1005\mathrm{J/KgK}$. For concrete, $\varphi = 0.05$ and $(\rho C)_s = 960\mathrm{J/KgK}$. Hence concrete-air

combination has $\varkappa = [\varphi(\rho C)_f + (1-\varphi)(\rho C)_s]/(\rho C)_f = 0.96$. Similarly, a closely packed bed of spherical glass beads of diameter 0.3 cm ($\varphi = 0.4$) filled with air has $\varkappa = 0.91$. Low density foam made up of polyurethane ($\varphi = 0.98$) saturated with air has $\varkappa = 0.998$. Moreover, we note that the kinematic viscosity of air at 30 °C is $\nu = 0.16 \times 10^{-4}$ m$^2$/s and the acceleration due to gravity is $g_0 = 9.81$ m/s$^2$. Hence a simple calculation shows that, if the layer is vibrating with the frequency $\Omega = 15$ Hz and amplitude $A = 0.15$ m, we obtain the nondimensional frequency $\omega$ as 23.438 and the nondimensional amplitude $\eta$ as 3.443, 34.438, and 344.387 for the porosity $\varphi = 1$, 0.1, and 0.01, respectively.

### A. Heated below (Ra > 0)

The dependence of $\mathrm{Ra}_c$ for small amplitude vibrations is plotted in Fig. 1 for a wide range of vibrating frequency. An increase in the conductivity ratio $\gamma$ in general advances the onset of convection. However, this trend is altered for very low $\omega$, which can be seen in the Darcy regime. Thus the presence of vibrations could lead to dual effects of $\gamma$ depending on the vibrating frequency as against the nonvibrating case, wherein $\gamma$ is always destabilizing [13]. It is also seen that the effect of $\gamma$ is more pronounced for its small values demonstrating the major influence of nonequilibrium phenomena. We notice that the LTE results are approached when $\gamma$ becomes 100 (see [24]). It was already demonstrated that the small amplitude

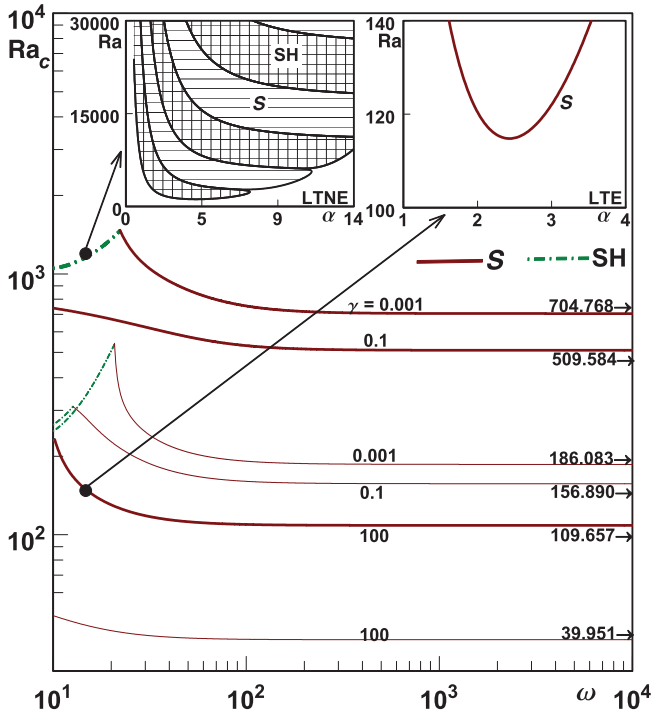


FIG. 1. (Color online) Heating from below in the presence of low amplitude ($\eta = 2$) vibrations. Dependence of $\mathrm{Ra}_c$ as a function of $\omega$ for $H = 100$ and different values of $\gamma$. Thin lines correspond to the results of the Darcy model and heavy lines correspond to the results of the Brinkman model. $\mathrm{Ra}_c \to \mathrm{Ra}_{0c}$ at sufficiently high frequency is marked in each curve. Insets show the marginal curves for LTE and LTNE; the presence of LTNE introduces the loop shaped marginal curves with $S$ and SH modes alternating each other.

restriction conceals a multilooped marginal curve, which is a characteristic of parametric excitation [24,26]. We now notice, from the insets, that the marginal curve corresponding to large $\gamma$ exhibits a single minimum, whereas that corresponding to small $\gamma$ shows a multiloop. Thus qualitative changes are introduced in the marginal curves even for small amplitude vibrations when the system exhibits thermal nonequilibrium.

Figure 1 shows that the onset of instability is of SH type for small values of $\gamma$ and $\omega$. As $\omega$ increases, it changes from SH to $S$ mode suddenly at a particular frequency (as low as $\omega = 25$ when $\gamma = 0.001$), called transition frequency, and continues to be the preferred one for higher frequencies however large. The corresponding $\mathrm{Ra}_c$ exhibits a cuspidal point at the transition frequency. The changes that took place in the marginal curves near the transition need special attention. Initially, the bottommost loop was SH for very small $\omega$. As $\omega$ started increasing toward the transition frequency, an additional thin $S$ loop emerged in the low wave-number region. Its minimum then reached the level of the already existing SH loop and hence $\mathrm{Ra}_c$ for both the $S$ and SH modes became equal at the transition frequency (bicritical situation). Thus, at this stage, $\alpha_c$ experienced a sudden jump to a lower value, indicating a catastrophic change in the length scale of the ensuing convection cells, $\lambda = 2\pi h/\alpha_c$. For a further increase in $\omega$ beyond this transition frequency, the $S$ mode grew further and became critical. It is to be mentioned at this stage that the convergence rate of $M_n$, $n = 0,1,2,\ldots$ in Eqs. (31) and (32) was found to increase against $\omega$. As many as 10 to 15 terms were required for lower values of $\omega$ against a maximum of five terms for higher values of $\omega$. The same trend was maintained throughout the present study with proportionately more number of terms for large amplitude vibrations. The stability limits in Fig. 1 beyond the transition frequencies, occurring at the low $\omega$ region, approach those of the nonvibrating case asymptotically. Thus the system is unable to react to vibrations at large frequencies. Also, we observe that there is no mode transfer for large $\gamma$ (LTE case) and the $S$ mode remains the preferred one throughout the frequency range under consideration.

The interplay between the $S$ and SH modes is apparent in Fig. 2 for an increased vibration amplitude. At low frequencies, we can see some cusps in $\mathrm{Ra}_c$ for smaller $\gamma$ representing the interaction between the two modes when the porous medium is away from thermal equilibrium. As $\omega$ increases further, the system is significantly stabilized via the SH mode, until a final transition frequency is reached and then destabilized rapidly via the $S$ mode to reach the nonvibrating limits. Also, we note that the jumps in $\alpha_c$ become wide at high frequencies. Moreover, we observed that, when the vibrational effect is felt, the augmentation of the onset of convection by $\gamma$ is via constricted patterns in contrast to $\eta = 2$, the nearly nonvibrating situation [13–15]. The Brinkman model is found to delay the onset compared to the Darcy model. This is because of the increased viscous resistance near the boundaries that opposes the fluid to move with ease. We observe that the boundary effect brought in by the Brinkman model shifts the final transition frequency to higher values, thereby extending the competition between the two modes over a wider region of $\omega$. On the other hand, an increase in $\gamma$ leaves the opposite effect. Hence the stability limits are markedly modified under

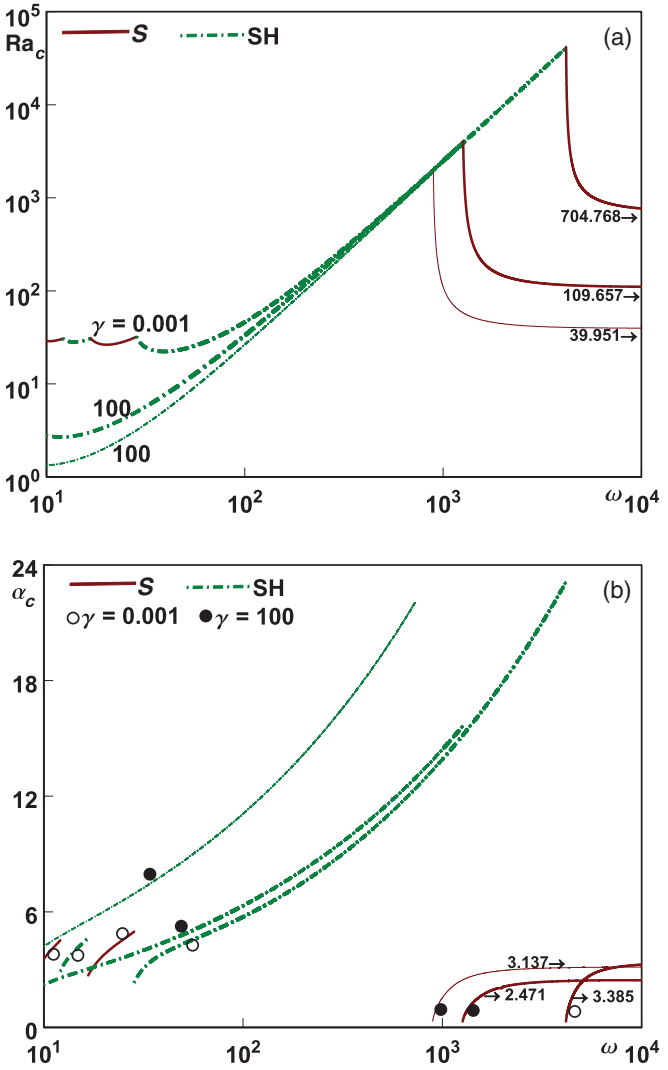


FIG. 2. (Color online) Heating from below in the presence of high amplitude ($\eta = 200$) vibrations. Dependence of (a) $\mathrm{Ra}_c$ and (b) $\alpha_c$ as a function of $\omega$ for $H = 100$ and different values of $\gamma$.

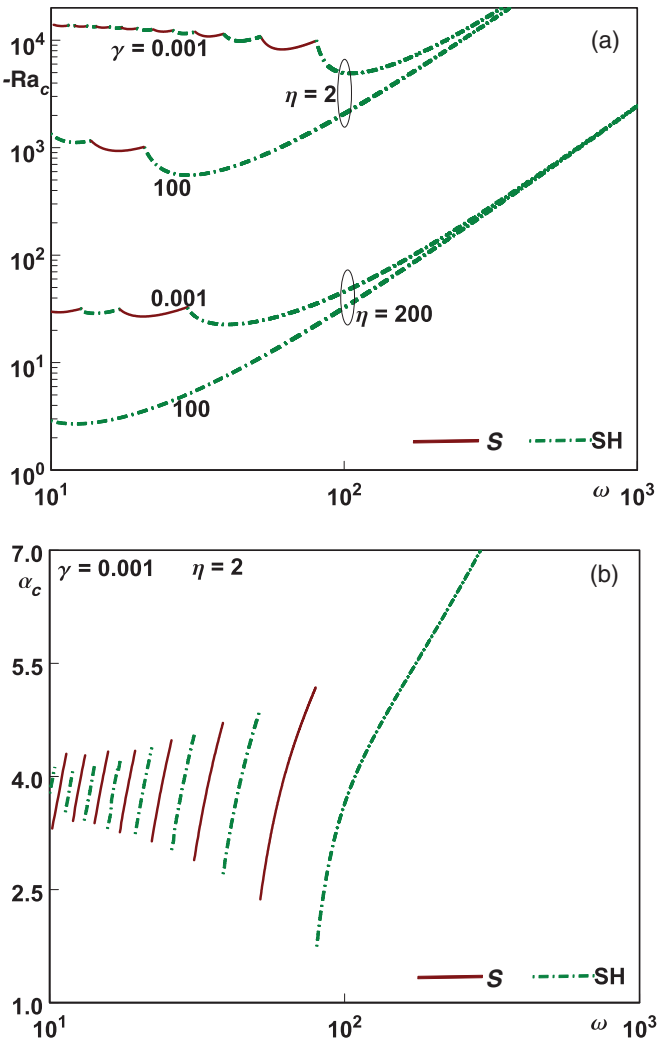


FIG. 3. (Color online) Heating from above. Dependence of (a) $\mathrm{Ra}_c$ and (b) $\alpha_c$ as a function of $\omega$ for $H = 100$ and different values of $\gamma$ and $\eta$. In (b), $\alpha_c$ shown only for $\eta = 2$ and $\gamma = 0.001$.

externally imposed vibrations as the porous medium starts showing thermal nonequilibrium.

### B. Heated above ($\mathrm{Ra} < 0$)

In the absence of mechanical vibrations, a layer heated from above is obviously stratified and thermally stable and hence no convection occurs. However, for sufficiently large temperature gradients, damped internal gravity waves exist, which can sustain for longer duration due to their large decay time compared to the temporal period. Hence convective instability can be triggered if there is a resonant coupling of these factors to the imposed external vibration.

The onset criteria for different values of $\gamma$ in the presence of both small and large amplitude vibrations are shown in Fig. 3. We observed that $-\mathrm{Ra}_c \to \infty$ for both $\omega \to 0$ and $\omega \to \infty$. At very low vibrating frequencies, it is impossible to destabilize the diffusive equilibrium state. This is the substantial physical reason for unboundedness of $-\mathrm{Ra}_c$ near $\omega = 0$. On the other extreme, when $\omega$ takes higher values, the porous layer starts behaving as if it is not forced to oscillate and hence the effect of gravity modulation dies down, similar to $\mathrm{Ra} > 0$. Moreover, the SH mode remains critical for $\omega > 10^2$. Hence we have restricted the upper limit of $\omega$ to $10^3$. From Fig. 3(a), we observe that the effect of $\gamma$ is unique, unlike the case of $\mathrm{Ra} > 0$. It advances the onset of motion, but always constricts the convective cells ensuing at the threshold for all vibrational amplitudes. For small values of $\gamma$, we observe a severe competition between the $S$ and SH modes over a wider range of $\omega$. The $S$ and SH branches become increasingly small and closely packed as the approach of $\omega$ is toward zero. The corresponding $\alpha_c$ depicted in Fig. 3(b) shows a possible yet sensitive control of convective pattern by tuning the forcing frequency. Also, we note that the jump in $\alpha_c$ is narrow at low frequencies and gradually widens as $\omega$ increases. We note that the effects of $\gamma$ are similar to those for $\mathrm{Ra} > 0$. They show that vibrations of larger amplitude leave a destabilizing effect. However, we notice that when the porous medium exhibits the LTE phenomenon, the instability is dictated solely by the SH response. Thus interaction between the $S$ and SH

modes comes into the picture as the medium starts moving away from thermal equilibrium. Unlike the case Ra > 0, the system was always observed to be more prone to instability, which manifests in the form of smaller cellular patterns for an increase in $\eta$ for all $\omega$.

### C. Effect of Pr

Figure 4 displays the effect of Pr for different values of Da and $H$. The stability limits approach those of the nonvibrating case via the $S$ mode for very small and large Pr limits (refer to [7,24]). However, it is clear that the SH mode becomes dominant for intermediate values of Pr creating two transitional Pr's. Nevertheless, in our previous study [24] based on the LTE assumption, the $S$ mode was observed to determine the critical condition throughout the range of Pr as Da $\to$ 0. Thus the effect of thermal nonequilibrium is to introduce subharmonic oscillations of the convective pattern for the Darcy regime as well. The critical Rayleigh number $\mathrm{Ra}_c$ decreases to its minimum value, while the critical wave number $\alpha_c$ attains its maximum value in the intermediate range of Pr. In other words, a critical Pr exists with the corresponding convective cells ensuing at the threshold reaching their smallest size. Also, we observe that the SH mode extends to a wider range of Pr as Da increases. Figure 4(b) shows that $\alpha_c$ exhibits different behaviors in the neighborhoods of the transitional Pr's. It decreases for the Brinkman model, whereas it increases abruptly for the Darcy model near the one occurring in the low Pr region. However, this trend reverses partially, depending on $c$, near the other occurring in the high Pr region. A clearer understanding of the situation can be obtained from the resonance regions at the marginal state for the Darcy model, shown in the inset, exhibiting an additional disconnected $S$ loop belonging to higher $\alpha$ becoming critical.

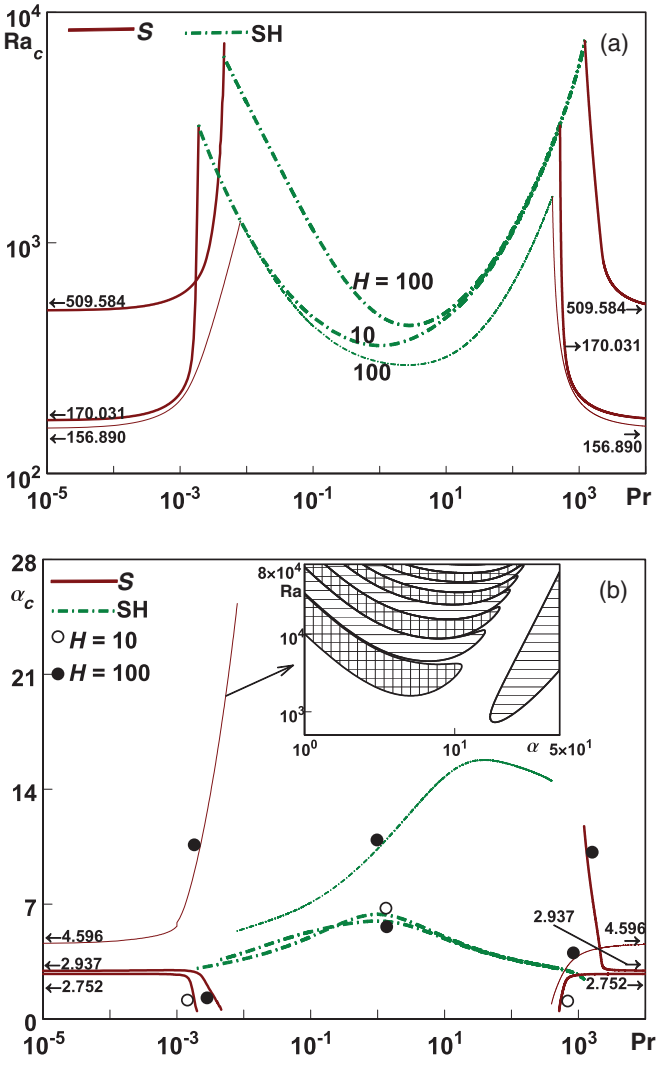


FIG. 4. (Color online) Heating from below. Dependence of (a) $\mathrm{Ra}_c$ and (b) $\alpha_c$ as a function of Pr for $\eta = 20$, $\omega = 100$, $\gamma = 0.1$, and different values of $H$. Inset in (b) shows the different topology of the marginal curves for Pr = 0.005.

### D. Effect of $H$

The influence of the interphase heat-transfer coefficient $H$ for different values of $\gamma$ and $\eta$ is shown in Fig. 5. We observe from Figs. 5(a) and 5(c) that, for $H \to 0$, $\mathrm{Ra}_c$ is independent of $H$ and $\gamma$. This is because very small values of $H$ correspond to a state in which the fluid and solid phases remain almost without any interaction and the fluid phase alone takes part in convection. In this situation, naturally even a high contrast in conductivities of the two phases has no effect. Similarly, for $H \to \infty$, both phases interact well and hence can be regarded as a single phase. Thus, in this case, also $\mathrm{Ra}_c$ was observed to be independent of $H$, which can be seen to a certain extent for $\omega = 10$ and $\eta = 200$. Thus $H$ leaves its effect on $\mathrm{Ra}_c$ only for its intermediate values, of course, depending on $\gamma$. This study almost reproduces the critical curves of the unmodulated problem for Ra > 0 [14,15] when $\omega = 1000$ and $\eta = 2$: $\mathrm{Ra}_c$ increases monotonically against $H$ and $\alpha_c$ increases, reaches a maximum, and then decreases against $H$, maintaining almost the same value for $H \to 0$ and $\infty$. However, $S$ mode remains critical throughout, as already mentioned in Sec. IV A. This behavior is altered and either the $S$ or SH mode emerges at the critical point for intermediate values of $H$ when the layer is exposed to mechanical vibrations. The corresponding $\alpha_c$ was also found to deviate from its LTE value only for intermediate values. These can be clearly seen when $\omega = 10$ and $\eta = 200$. It is also noticed that when both the vibration parameters assume higher values, then the interaction between the two phases is suppressed for a wider range of $H$.

In the case of heating from above, one can see $-\mathrm{Ra}_c \to \infty$ in the LTE limit when the layer is nearly unmodulated, i.e., when $\omega = 1000$ and $\eta = 2$. This is obvious because of the thermally stable background state. An interesting behavior in the non-LTE regime, which was not seen for Ra > 0, is the existence of a severe competition between the $S$ and SH modes for intermediate values of $H$. One can also observe from Fig. 5(c) that an increased $\omega$ suppresses thermal interaction between the fluid and solid phases for a wider range of $H$. The behavior of $\alpha_c$ for intermediate values of $H$ is completely different from that of a nonvibrating porous layer with LTNE effect. It decreases, reaches a minimum, and then increases against $H$. It also exhibits a catastrophic jump at each mode transition. It is also clear from Fig. 5 that when $\eta = 200$,

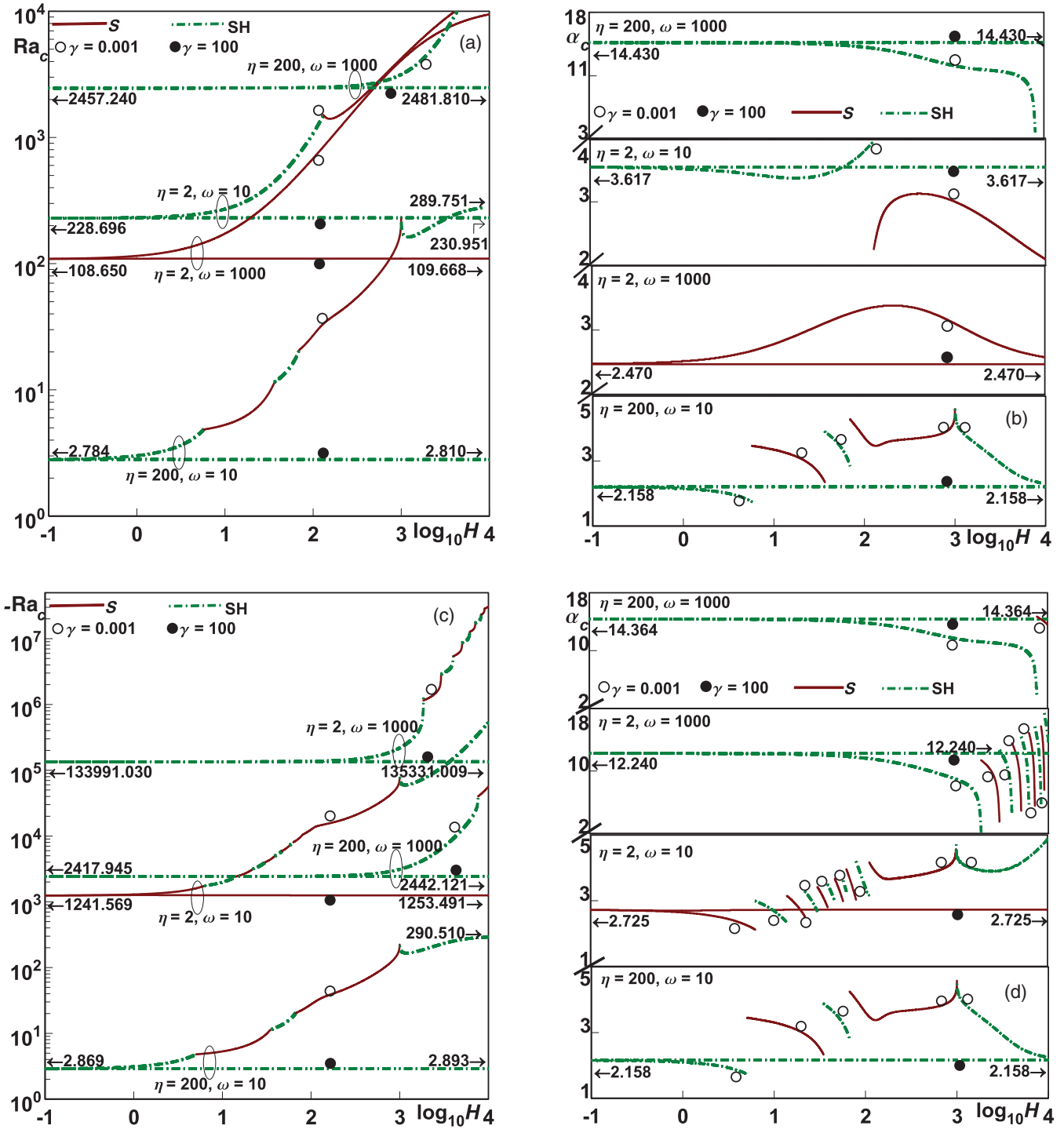


FIG. 5. (Color online) Heating from below. Dependence of (a) $\mathrm{Ra}_c$ and (b) $\alpha_c$ as a function of $H$ for different values of $\gamma$, $\eta$, and $\omega$. $\mathrm{Ra}_c \to \mathrm{Ra}_{0c}$ and $\alpha_c$ at $H \to 0$ and $H \to \infty$ are marked in each curve. Heating from above. Dependence of (c) $\mathrm{Ra}_c$ and (d) $\alpha_c$ as a function of $H$ for different values of $\gamma$, $\eta$, and $\omega$. $\mathrm{Ra}_c \to \mathrm{Ra}_{0c}$ and $\alpha_c$ at $H \to 0$ and $H \to \infty$ are marked in each curve.

both $|\mathrm{Ra}_c|$ and $\alpha_c$ are almost the same. Thus we arrive at the significant result that vibrations with higher amplitude have the same effect whether the layer is heated from below or from above. A similar result was predicted in the LTE case also [24]. In general, it is seen from Fig. 5 that mechanical vibration does not alter the general pattern of $\mathrm{Ra}_c$ curves corresponding to the nonvibrating porous medium using LTNE, but the convective cells at the threshold exhibit different behavior.

### E. Experimental validation

Before concluding this section, we would like to present a comparison of the linear stability results with the available laboratory observations of Rogers *et al.* [8]. To do this, we assumed $K \to \infty$ and $\varphi = 1$ corresponding to a clear fluid and the layer to be confined between rigid surfaces. This requires $u_3 = Du_3 = \theta = \phi = 0$ at the surfaces. For this, we used the first-order Galerkin approach as in [24]. Accordingly,

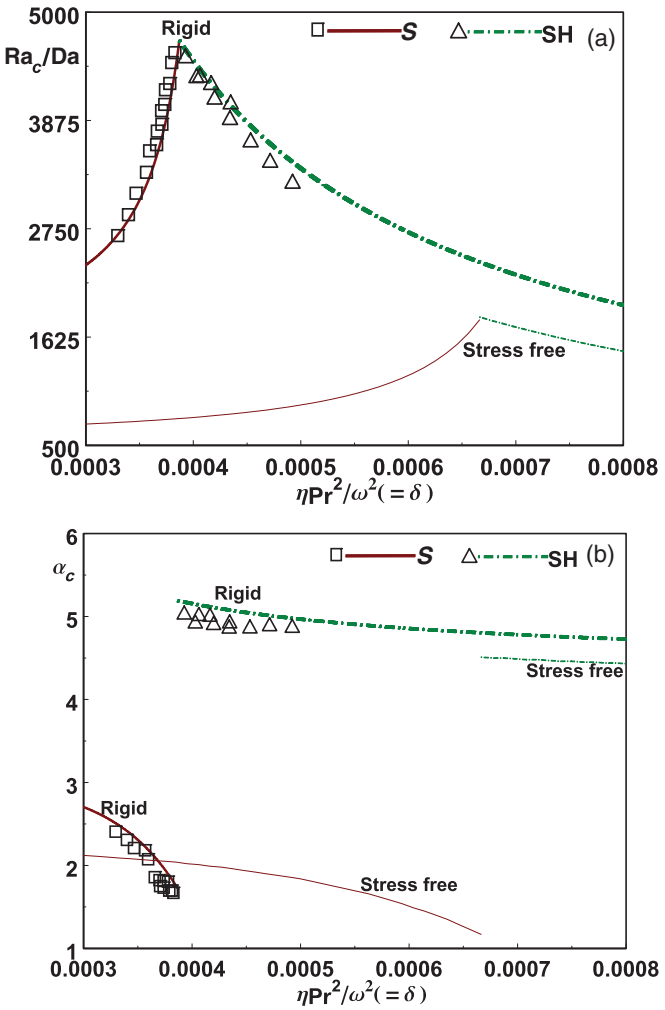


FIG. 6. (Color online) Comparison of (a) $Ra_c$ and (b) $\alpha_c$ with Rogers *et al*. [8] for the clear fluid case.

we represented $\widehat{u_3}(z,t) = a_1(z)F(t)$, $\widehat{\theta}(z,t) = a_2(z)\Theta(t)$, and $\widehat{\phi}(z,t) = a_3(z)\Phi(t)$ in Eqs. (15)–(17) with the trial functions $a_1(z) = z^2(1-z)^2$ and $a_2(z) = a_3(z) = z(1-z)(1+z-z^2)$. The results given in [8] are for $Pr = 0.93$ and their vibrating frequency, $\omega' = 98$. Owing to the use of different scalings, the vibrating parameters in the present study are related to their counterparts $\omega'$ and $\delta'$ of [8] as $\omega = \omega'/Pr$ and $\delta = \eta/\omega'^2$. Figure 6 shows the identical qualitative natures of the critical limits for rigid and stress-free boundaries. We also notice a very good agreement with the experimental results validating the numerical procedure adopted.

## V. CONCLUSION

The influence of relaxing the LTE assumption on the stability of a horizontal fluid saturated porous layer is examined under time-periodic vertical vibrations. The temperature gradient imposed across the layer may be either parallel or antiparallel to the gravity field. The flow through the porous medium is governed by Brinkman's law. The following findings are obtained.

The nonequilibrium effect is felt only for intermediate values of $H$ depending on $\gamma$, Da, $\omega$, and $\eta$; $H$ stabilizes the system.

The effect of $\gamma$ is to advance the onset of motion. It constricts the convective cells ensuing at the threshold, except when the layer heated from below is subjected to small amplitude vibrations.

The competition between the $S$ and SH modes becomes significant when $\gamma$ assumes smaller values. It is found to occur over a wider range of $\omega$ when Da takes higher values. However, this coupling cannot be observed for small amplitude vibrations.

In the case of $Ra > 0$, the interaction between the two phases is suppressed for a wider range of $H$ when both $\omega$ and $\eta$ are large. However, in the case of $Ra < 0$, the suppression is found when $\omega$ takes higher values irrespective of $\eta$.

Vibrations of larger amplitude do not influence the onset conditions significantly when the layer is heated from above. They have the same effect for both $Ra > 0$ and $Ra < 0$.

In contrast to the LTE situation [24], the LTNE introduces the SH mode for intermediate values of Pr irrespective of the value taken by Da.

## ACKNOWLEDGMENTS

The authors thank University Grants Commission, India for its support through DRS Special Assistance Programme in Fluid Dynamics. This work was carried out as a part of a research project [Grant No. 25(0169)/09/EMR-II] awarded by Council of Scientific and Industrial Research, India. Its financial assistance to one of the authors (T.S.) is gratefully acknowledged.

[1] H. Bénard, Ann. Chim. Phys. **7**, 62 (1901).
[2] M. C. Cross and P. C. Hohenberg, Rev. Mod. Phys. **65**, 851 (1993).
[3] M. Faraday, Philos. Trans. R. Soc. London **121**, 299 (1831).
[4] P. M. Gresho and R. L. Sani, J. Fluid Mech. **40**, 783 (1970).
[5] G. Z. Gershuni, E. M. Zhukhovitskii, and I. S. Iurkov, J. Appl. Math. Mech. **34**, 442 (1970).
[6] R. Clever, G. Schubert, and F. H. Busse, J. Fluid Mech. **253**, 663 (1993).
[7] S. Aniss, M. Souhar, and M. Belhaq, Phys. Fluids **12**, 262 (2000).
[8] J. L. Rogers, M. F. Schatz, J. L. Bougie, and J. B. Swift, Phys. Rev. Lett. **84**, 87 (2000).
[9] K. K. Gabdrakhmanov, G. Z. Gershuni, E. M. Zhukhovitskii, and V. G. Kozlov, Izv. Acad. Sci. USSR, Atmos. Oceanic Phys. **26**, 1315 (1990).
[10] V. G. Kozlov, Fluid Dyn. **37**, 536 (2002).
[11] D. A. Nield and A. Bejan, *Convection in Porous Media* (Springer-Verlag, New York, 2006).
[12] D. A. S. Rees and I. Pop, in *Local Thermal Nonequilibrium in Porous Medium Convection*, Transport Phenomena in Porous Media III, edited by D. B. Ingham and I. Pop, Chap. 6 (Elsevier, New York, 2005).
[13] N. Banu and D. A. S. Rees, Int. J. Heat Mass Transf. **45**, 2221 (2002).

[14] A. Postelnicu and D. A. S. Rees, Int. J. Energy Res. **27**, 961 (2003).
[15] M. S. Malashetty, I. S. Shivakumara, and K. Sridhar, Int. J. Heat Mass Transf. **48**, 1155 (2005).
[16] A. Postelnicu, Int. J. Therm. Sci. **47**, 1587 (2008).
[17] B. Straughan, Proc. R. Soc. London, Ser. A **462**, 409 (2006).
[18] M. S. Malashetty, S. Mahantesh, and K. Sridhar, Phys. Fluids **19**, 054102 (2007).
[19] A. Nouri-Borujerdi, A. R. Noghrehabadi, and D. A. S. Rees, Transp. Porous Media **69**, 343 (2007).
[20] S. Saravanan, Transp. Porous Media **76**, 35 (2009).
[21] A. Postelnicu, Int. J. Heat Mass Transf. **53**, 68 (2010).
[22] A. V. Kuznetsov and D. A. Nield, Transp. Porous Media **83**, 425 (2010).
[23] Y. P. Razi, K. Maliwan, M. C. Mojtabi, and A. Mojtabi, in *The Influence of Mechanical Vibrations on Buoyancy Induced Convection in Porous Media*, Handbook of Porous Media, edited by K. Vafai, Chap. 8 (Taylor & Francis, London, 2005).
[24] S. Saravanan and T. Sivakumar, Phys. Fluids **22**, 034104 (2010).
[25] S. Saravanan and A. Purusothaman, Int. J. Therm. Sci. **48**, 2085 (2009).
[26] S. Saravanan and T. Sivakumar, ASME J. Heat Transfer **133**, 051601 (2011).
[27] M. S. Malashetty and V. Padmavathy, Int. J. Eng. Sci. **35**, 829 (1997).
[28] G. S. Markman and V. I. Yudovich, Fluid Dyn. **7**, 434 (1972).
[29] Y. P. Razi, A. Mojtabi, and M. C. Charrier-Mojtabi, Trans. Porous Media **77**, 207 (2009).
[30] N. Strong, J. Math. Fluid Mech. **10**, 488 (2008).
[31] K. Walker and G. M. Homsy, ASME J. Heat Transfer **99**, 338 (1977).